Two-Dimensional Electromagnetic Solver Based on Deep Learning Technique

Shutong Qi, Yinpeng Wang, Yongzhong Li, Xuan Wu, Qiang Ren, and Yi Ren, *Member, IEEE*

***Abstract*—Although the deep learning technique has been introduced into computational physics in recent years, the feasibility of applying it to solve electromagnetic (EM) scattering field from arbitrary scatters remains open. In this article, the convolutional neural network (CNN) has been employed to predict the EM field scattered by complex geometries under plane-wave illumination. The 2-D finite-difference frequency-domain (FDFD) algorithm, wrapped by a module to randomly generate complex scatters from basic geometries, is employed to produce training data for the network. The multichannel end-to-end CNN is modified and combined with residual architecture and skip connection, which can speed up convergence and optimize network performance, to form the EM-net. The well-trained EM-net has good performance in this problem since it is compatible with different shapes, multiple kinds of materials, and different propagation directions of the incident waves. The effectiveness of the proposed EM-net has been validated by numerical experiments, and the average numerical error can be as small as 1.23%. Meanwhile, its speedup ratio over the FDFD method is as large as 2000.**

***Index Terms*—Convolutional neural network (CNN), deep learning, finite-difference frequency-domain (FDFD) method, 2-D Maxwell's equation.**

I. Introduction

COMPUTATIONAL electromagnetics (CEM) plays an important role in both academic research and industrial engineering, such as antenna design, geophysical exploration, space remote sensing, and other related fields. The classical methods in CEM include finite-element methods (FEM) [1], finite-difference methods (FDM) [2], method of moments (MoM) [3], etc. These methods usually partition the geometries into large quantity of elements and construct corresponding equations of matrices on the mesh according to the excitation and the boundary conditions. No matter whether direct or iterative solvers [4] are employed, it is computationally cumbersome to these equations, which will lead to high memory usage and long CPU time.

Thanks to the rapid development of big data science and high-performance computing, the deep learning (DL) technique reveals potential in varieties of applications, such as natural language processing [5], image classification [6], [7], image segmentation [8]–[10], human-centered robotics [11], antenna array design [12], etc. These applications have replaced boring repetitive tasks accurately and efficiently.

It is a natural and straightforward question whether the DL technique can be implanted to the realm of computational physics. If the physical interaction between the incident wave and the scatter (or the medium) can be approximated by a network instead of algebra equations of matrices, the computational load is, at least for the online evaluation, expected to be decreased significantly. Many researchers have obtained meaningful and inspiring results.

In computational fluid dynamics (CFD) area, convolutional neural network (CNN) is used to replace computationally expensive CFD solvers to approximate the real-time velocity field [13] and accelerate the Navier–Stokes equations to model liquid behavior with obstacles [14]. In [15], a large-scale Poisson system has also been solved successfully by CNN combined with a principle component analysis process.

In CEM, some pioneering work has been reported. In [16] and [17], the 2-D and 3-D electrostatic problems have been solved, respectively, by using CNN. In electrodynamic modeling, the MoM solver has been replaced by a simple multilayer artificial neural network (ANN) and the finite-difference frequency-domain (FDTD) solver has been replaced by a combination of CNN and recurrent neural network, as described in [18] and [19]. Furthermore, the perfectly matched layer of the FDTD method has been accelerated by the ANN [20]. In [21], CNN has been applied to predict the solution of Maxwell's equations for low-frequency EM devices. Recently, CNN has been proposed to solve EM inverse scattering problems [22]–[24]. However, among the computational physics solvers based on the DL technique, parameter basis solvers always have limited scope of application while pixel basis solvers prefer the time-domain problems. Few works have tried to get the vector result of arbitrary scatters' EM field on the pixel basis in the frequency domain.

In this article, we investigate the feasibility of applying the DL technique to replace the conventional 2-D full-wave electrodynamic solver for scattering problems. First, a 2-D efficient

Manuscript received November 29, 2019; revised January 23, 2020 and March 19, 2020; accepted May 14, 2020. Date of publication May 19, 2020; date of current version June 4, 2020. This work was supported in part by the National Natural Science Foundation of China under Grant 61801009 and Grant 61871063, and in part by the 13th Five-Year Equipment Pre-Research Fund under Grant 61402090603 and Grant 61402080205. *(Shutong Qi and Yinpeng Wang contributed equally to this work.) (Corresponding authors: Qiang Ren; Yi Ren.)*

Shutong Qi, Yinpeng Wang, Yongzhong Li, Xuan Wu, and Qiang Ren are with the School of Electronic and Information Engineering, Beihang University, Beijing 100191, China (e-mail: tony0612@buaa.edu.cn; 16081072@buaa.edu.cn; liyongzhong@buaa.edu.cn; dearpony@buaa.edu.cn; qiangren@buaa.edu.cn).

Yi Ren is with the School of Electronic Engineering, Chongqing University of Posts and Telecommunications, Chongqing 400065, China (e-mail: renyi_cq@hotmail.com).

Digital Object Identifier 10.1109/JMMCT.2020.2995811

FDFD solver is employed as the core of the forward modeling code and its effectiveness has been validated via comparison to the commercial software package COMSOL Multiphysics. Then, this FDFD core has been wrapped by a complex geometry generation module, in which typical 2-D shapes (circles, ellipses, and polygons) are remixed to form complex ones. Two images, one representing the incident wave and the other containing the scatter, are the input of the network. U-Net [9], which is based on U-network approach, was first developed to tackle segmentation problems in biomedical image processing, and further demonstrated its robustness in image prediction where input and output pairs are spatially correlated. Herein, we report an end-to-end CNN which integrates U-network and residual [25] architecture to provide accurate EM field estimation. Thanks to the residual blocks, this proposed network has good convergence performance even if it has more than 70 layers. The well-trained EM-net can evaluate the scattered EM fields and fit various kinds of shapes' EM field at an average error rate of 1.23%. More importantly, it only takes about 20 ms on average to calculate one sample, which is 2000 times faster than conventional FDFD method. Also, complex scatters do not lead to an increase of the computation time.

This article is organized as follows. In Section II, the FDFD solver and the scatter generating module are exhibited, followed by the description of the proposed network and how the network can replace a conventional FDFD full-wave solver. In Section III, the proposed framework is validated via numerical experiments, high accuracy and efficiency are confirmed, and developing experiments have been conducted to explore the well-trained network's generality. The conclusion is given in Section IV.

II. Methods and Formulations

The FDFD solver is implemented, and its effectiveness is verified by comparing to the commercial software COMSOL Multiphysics. This solver is further combined with a random geometry generator to obtain the total EM field data from a large number of scatters. The data are used to train and test the proposed neural network.

A. Finite-Difference Frequency-Domain Method

The finite-difference method is a method to build a solvable difference equation out of differential equations by approximating the derivatives in each computation region.

The frequency domain Maxwell equations are as follows:

$$\nabla \times \boldsymbol{E} = -i\omega\mu\boldsymbol{H} \tag{1}$$

$$\nabla \times \boldsymbol{H} = i\omega\varepsilon\boldsymbol{E} + \boldsymbol{J} \tag{2}$$

where $\boldsymbol{E}$ and $\boldsymbol{H}$ are the intensity of electric and magnetic fields, $\boldsymbol{J}$ is the electric current source, and ε and μ are the permittivity and permeability, respectively.

By approximating the derivatives with central difference scheme in Cartesian coordinates, the first-order frequency-domain Maxwell's equation can be transformed into six scalar equations as

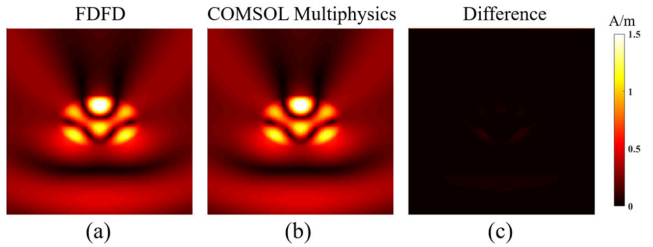

Fig. 1. Distribution of (a) $|H_z|$ from FDFD and (b) $|H_z|$ from COMSOL Multiphysics. (c) Difference of $|H_z|$ between FDFD and COMSOL multiphysics.

$$\frac{E_z^{i,j+1,k} - E_z^{i,j,k}}{\Delta_y^j} - \frac{E_y^{i,j,k+1} - E_y^{i,j,k}}{\Delta_z^k} = -i\omega\mu_x^{i,j,k} H_x^{i,j,k} \tag{3}$$

$$\frac{E_x^{i,j,k+1} - E_x^{i,j,k}}{\Delta_z^k} - \frac{E_z^{i+1,j,k} - E_z^{i,j,k}}{\Delta_x^i} = -i\omega\mu_y^{i,j,k} H_y^{i,j,k} \tag{4}$$

$$\frac{E_y^{i+1,j,k} - E_y^{i,j,k}}{\Delta_x^i} - \frac{E_x^{i,j+1,k} - E_x^{i,j,k}}{\Delta_y^j} = -i\omega\mu_z^{i,j,k} H_z^{i,j,k} \tag{5}$$

$$\frac{H_z^{i,j,k} - H_z^{i,j-1,k}}{\tilde{\Delta}_y^j} - \frac{H_y^{i,j,k} - H_y^{i,j,k-1}}{\tilde{\Delta}_z^k} = i\omega\varepsilon_x^{i,j,k} E_x^{i,j,k} + J_x^{i,j,k} \tag{6}$$

$$\frac{H_x^{i,j,k} - H_x^{i,j,k-1}}{\tilde{\Delta}_z^k} - \frac{H_z^{i,j,k} - H_z^{i-1,j,k}}{\tilde{\Delta}_x^i} = i\omega\varepsilon_y^{i,j,k} E_y^{i,j,k} + J_y^{i,j,k} \tag{7}$$

$$\frac{H_y^{i,j,k} - H_y^{i-1,j,k}}{\tilde{\Delta}_x^i} - \frac{H_x^{i,j,k} - H_x^{i,j-1,k}}{\tilde{\Delta}_y^j} = i\omega\varepsilon_z^{i,j,k} E_z^{i,j,k} + J_z^{i,j,k} \tag{8}$$

where $(i,\ j, k)$, $\varepsilon_w^{i,j,k}$, and $\mu_w^{i,j,k}$ denote the index, the permittivity, and permeability of the cell, respectively, and $\tilde{\Delta}_w^l = \frac{(\Delta_w^l + \Delta_w^{l-1})}{2}$, $(w = x,\ y,\ z)$.

The differential equations from all grid cells are collected to build the system equations

$$\boldsymbol{C}_e\boldsymbol{e} = -i\omega\boldsymbol{D}_\mu\boldsymbol{h} \tag{9}$$

$$\boldsymbol{C}_h\boldsymbol{h} = i\omega\boldsymbol{D}_\varepsilon\boldsymbol{e} + \boldsymbol{j} \tag{10}$$

where $\boldsymbol{C}_e$ and $\boldsymbol{C}_h$ are matrices for the curl operators on $\boldsymbol{E}$ and $\boldsymbol{H}$, respectively, and $\boldsymbol{D}_\mu$ and $\boldsymbol{D}_\varepsilon$ are diagonal matrices for the permeability and permittivity. After eliminating $\boldsymbol{e}$, the system of equations with single field unknown $\boldsymbol{h}$ is as follows:

$$\left(\boldsymbol{C}_h - \omega^2\boldsymbol{D}_\varepsilon\boldsymbol{C}_e{}^{-1}\boldsymbol{D}_\mu\right)\boldsymbol{h} = \boldsymbol{j}. \tag{11}$$

Direct solver or iterative solvers [26], [27] can be employed to obtain the solution.

Fig. 1 shows the comparison between FDFD and COMSOL multiphysics. The domain area is a square with the edge length

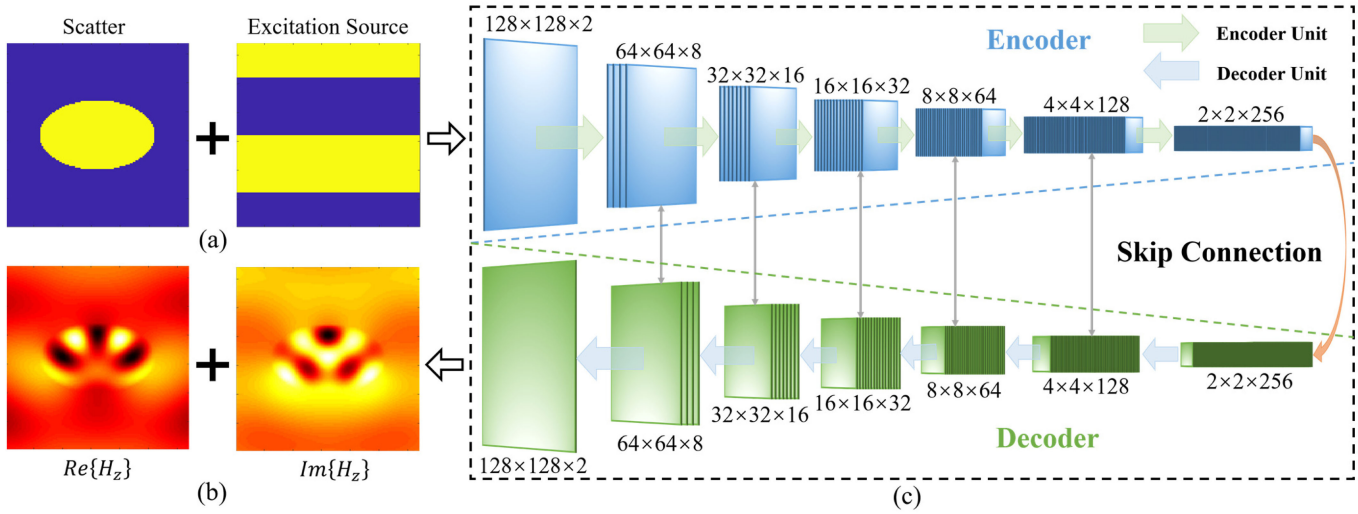

Fig. 2 Input, output, and structure of the EM-net. (a) Two input images representing scatter and source, respectively. (b) Two output images representing the real and imaginary parts of the predicted H_z. (c) Structure of the proposed network.

of 128 nm. The square is partitioned into 128×128 grids. The scatter is an ellipse located in the center of the domain with the major axis parallel to the horizontal direction. The semimajor axis of the ellipse is 30 nm and the eccentricity is 0.8. The excitation source is TE plane wave propagating along the *y*-axis and polarizing along the *x*-axis. The wavelength of the excitation source is 80 nm. From this comparison, we can see that the solution of FDFD is accurate. Then, the FDFD solver is wrapped by a random geometry generator to produce a large quantity of training data.

B. Network

Without loss of generality, the excitation source is assumed to be a TE plane wave with arbitrary propagation direction. In this article, the deep neural network is employed to approximate the inverse of the system matrix in (11), i.e.,$(\boldsymbol{C}_h - \omega^2 \boldsymbol{D}_\varepsilon \boldsymbol{C}_e{}^{-1} \boldsymbol{D}_\mu)^{-1}$ accurately. As Fig. 2(b) shows, the output from the network are two images which represent the real and imaginary parts of H_z.

To realize pixel basis image generation, we constructed CNN with a modified end-to-end pipeline. Since both the input and output of as-proposed network are images, it is convenient and flexible for various image production problems such as image segmentation and image reconstruction. But the original U-Net has limited fitting ability for this problem. Toward this case, the relative error compared with conventional physics solver under certain input is a vital evaluation standard. To increase U-Net's fitting ability, additional blocks and layers are highly required to be further added. However, as the complexity increases, it is hard to train the network and the results are far from satisfactory. Therefore, residual architecture is combined with the modified U-Net architecture to form an encoder–decoder structure, along with a skip connection to convey necessary global information. With these improvements, the proposed network (named EM-net) can perform pixel-based end-to-end data training.

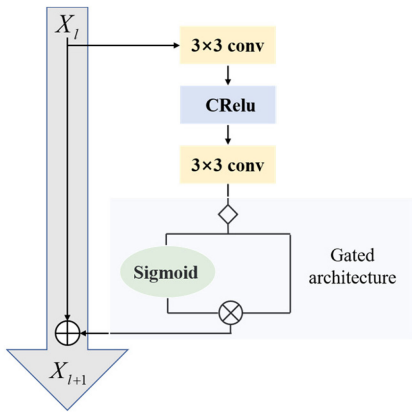

Fig. 3. Architecture of residual block in the encoder process.

The structure of the EM-net is shown in Fig. 2(c). The EM-net has six encoder units and six decoder units. Between the encoder and the decoder, there is also a full-connection unit. There are two residual blocks in each encoder unit and one in each decoder unit. One residual block has four layers, so eight layers are in each encoder unit and four layers are in each decoder unit. The full-connection unit also has four layers. There are eight filters in each layer and the kernel size is 3×3.

Fig. 3 shows the architecture of the residual block in the encoder process. X_l and X_{l+1}represent the input and output of the residual block, respectively. CRelu is applied to be the nonlinearity function. Passing CRelu function, the input dimension will be doubled. Then, the gated architecture will extract the linear and nonlinear features. All features combined with the original input will be mixed as output. Replacing convolution to transposed convolution is the residual block in the decoder process. The residual block can help extend the base in the backpropagation process, which will help pronounce the gradient.

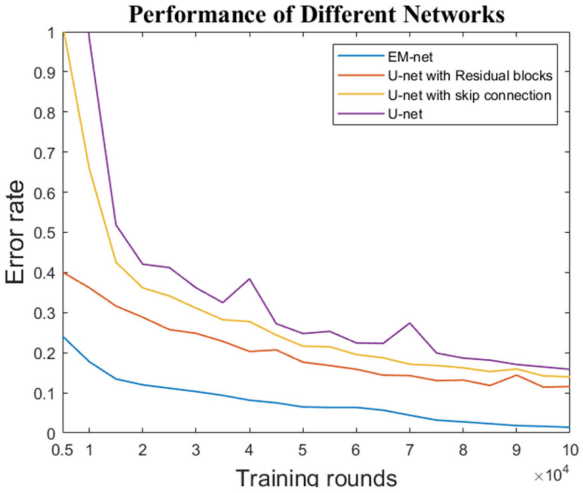

Fig. 4. Performance comparison between different networks.

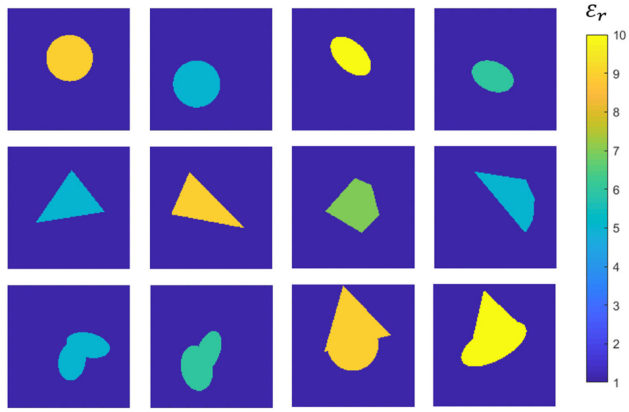

Fig. 5. Scatters of circles, ellipses, and polygons and their combinations with variable permittivity ranging from 2 to 10. The background medium is vacuum.

The encoder is a CNN with residual block which can map the inputting scatters into high-dimensional spatial representation with geometric features. While the decoder is a transposed convolutional network with residual block that rebuilds these features and restores it to the original image size. In the encoding process, due to the change of the dimensions, the global information of image is lost, which is important to the decoding process. Therefore, we use the skip-connection structure to convey the global information from the encoder unit to the corresponding decoder unit. In this way, the fitting ability of the network can be further improved.

In this article, the loss function can be expressed as

$$L = \frac{1}{2}\sum_{i}^{N}\sum_{j}^{N}\left(h\left(i,j\right)-g\left(i,j\right)\right)^2 \tag{12}$$

where g indicates the output of network, and h represents the ground truth calculated by the FDFD program.

The effectiveness of residual block and skip connection are verified through a set of experiments. In these experiments, original U-Net, U-Net with residual block, U-Net with skip connection, and our proposed network are trained to predict the same dataset. Fig. 4 shows how the error rate changes as the experiment proceeds. From these experiments, we can see that our proposed network has the best performance in terms of the final error rate and the convergence speed. Residual blocks make the model easier to converge and skip connection can further decrease the error rate of the well-trained network.

III. Numerical Results

In this article, the computational region is a square with the edge length of 128 nm. The square is partitioned into 128×128 grids. The direction of the illumination wave is arbitrary and its wavelength is 80 nm. In the numerical experiment, the amplitude of the illumination wave is set to be 200 V/m. The shapes of the scatters include simple geometric figures (circles, ellipses, triangles, and pentagons) and combination figures (two different ellipses, polygon, and ellipse), each of which accounts for one-sixth of the total dataset. Scatters are located randomly in the region. The circle has a radius ranging from 13 to 28 nm. The semimajor axis of the ellipse ranges from 19 to 26 nm, and the eccentricity ranges from 0.65 to 0.95. The chord of triangles and pentagons ranges from 32 to 64 nm. The background medium is vacuum and the scatter permittivity is randomly selected from [2]–[10]. Of the 36 000 sets of data, 90% are training sets and the others are testing sets.

Two images are used to store the information of the scatters and the source, which are shown in Fig. 2(a). In the scatter image, the value of each pixel is the relative permittivity of the material at this location. Several scatters are shown in Fig. 5. In the source image, the values of 1 and 0 indicate that the phase of the illumination plane wave at this location is in the range of [0, π) and [$-\pi$, 0), respectively. Since the phase of plane wave changes from positive to negative near the zero-phase point in the propagation direction and we fix this point at the center of the square, the propagation direction of the wave can be easily obtained from the image (from yellow to blue at the center of the square).

Fig. 6 shows several results randomly chosen from the testing cases. It can be observed that the predicted H_z agrees well with those computed by the FDFD method. The relative errors are also calculated to numerically evaluate the accuracy of the EM-net. The average relative error of each testing case can be expressed as

$$\text{error}_{\text{rate}} = \frac{1}{N^2}\frac{\sum_i^N\sum_j^N\left|H_{\text{network}}\left(i,j\right)-H_{\text{FDFD}}\left(i,j\right)\right|}{\sum_i^N\sum_j^N\left|H_{\text{FDFD}}\left(i,j\right)\right|} \times 100\% \tag{13}$$

where H_{network} and H_{FDFD} represent the complex-valued magnetic field from EM-net and FDFD, respectively, and N represents the number of grids on each side of the square.

The error distribution of testing sets is presented in Table I. The final average relative error from the EM-net is only 1.23%, which indicates that the EM-net has excellent prediction ability. Additionally, it only takes this neural network 20.8 ms on

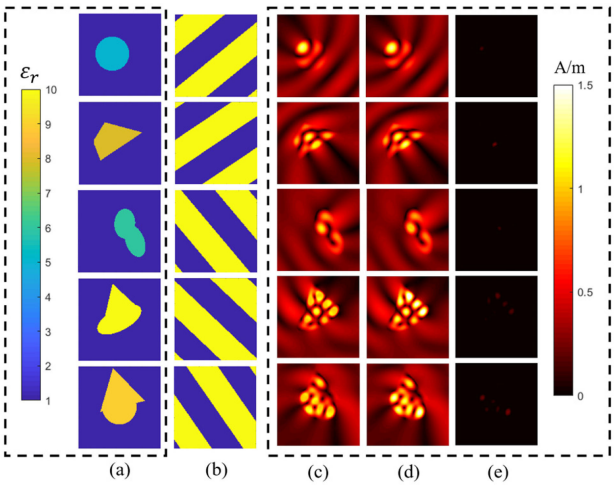

Fig. 6. Numerical examples to show the good performance of the EM-net. (a) Geometry and permittivity of the scatters. (b) Input images of the illumination plane waves. (c) Amplitude of H_z from the neural network. (d) Amplitude of H_z from the FDFD solver. (e) Error distribution.

TABLE I
RELATIVE ERROR OF TESTING SETS

Scatter	Single graphics	Combination	All scatters
Relative Error [%]	1.034	1.428	1.230

average to predict the magnetic field. In contrast, it spends approximate 40 s by using FDFD method (including the time to generate the mesh and assemble the system matrices).

After this experiment, the model's generality to scatter shapes and material is also explored. Quadrangles and hexagons, which do not exist in the training process, are used to test the well-trained model's generality to scatter shapes. The error rate of this developing experiment is 3.782%. In the experiment to explore the model's generality to material, the scatter's relative permittivity is an arbitrary floating-point number from 2 to 10. The average error rate of this experiment is 8.6%.

These experiments show that well-trained EM-net has good generality to the scatter shapes. But if scatter's relative permittivity is beyond the scope, the network performance will be degraded. It is because the diversity of the training data determines the scope of the network. If the network does not learn how to react to the change of any parameter, it will not feedback an expected result.

With the help of DL technique, a super-fast forward modeling CNN is built. It can accurately predict the magnetic fields scattered by complex geometries of various permittivity under the illumination of TE plane wave from any direction. Compared to the full-wave EM solver, such as the FDFD, the EM-net has much higher efficiency. It can be used in the applications in which real-time calculation is essential.

IV. CONCLUSION

In this article, an end-to-end CNN, which consists of U-network and residual architecture, has been applied to accelerate the solution of 2-D Maxwell's equations. This method is divided into two stages—offline training and online testing. In the offline stage, the FDFD method is employed to generate the dataset to train the network. As the training stage proceeds, the network will automatically change its nonlinear structure and finally, replace the equation in the FDFD solving process with a set of parameters. In the online part, two images, which represent the excitation plane wave and the scatter, respectively, are input into the network. Then, the network will output the total magnetic field according to the learning parameters.

From the results of the numerical experiments, the following conclusions can be drawn. First, the DL technique can be used to solve electrodynamic problems accurately and its generalization ability is good, which allows various materials and arbitrary plane-wave propagation directions. Second, residual blocks are of vital importance to the network with plenty of layers, and it can accelerate complex network convergence in the offline training stage and optimize the well-trained network performance. Third, the as-proposed CNN can significantly accelerate the solving process compared to the full-wave solver, which is more suitable for real-time evaluation.

REFERENCES

[1] J.-M. Jin, *The Finite Element Method in Electromagnetics*, 3rd ed. Hoboken, NJ, USA: Wiley-IEEE Press, 2014.
[2] A. Taflove and S. C. Hagness, *Computational Electrodynamics: The Finite-Difference Time-Domain Method*, 3rd ed. Norwood, MA, USA: Artech House, 2005.
[3] R. F. Harrington, *Field Computation by Moment Methods*. Hoboken, NJ, USA: Wiley-IEEE Press, 1993.
[4] G. H. Golub and C. F. V. Loan, *Matrix Computations*, 3rd ed. Baltimore, MD, USA: The Johns Hopkins Univ. Press, 1996.
[5] S. K. A. Fahad and A. E. Yahya, "Inflectional review of deep learning on natural language processing," in *Proc. Int. Conf. Smart Comput. Electron. Enterprise*, Shah Alam, Malaysia, 2018, pp. 1–4.
[6] A. Krizhevsky, I. Sutskever, and G. E. Hinton, "ImageNet classification with deep convolutional neural networks," in *Proc. 25th Int. Conf. Neural Inf. Process. Syst.*, 2013, pp. 1097–1105.
[7] O. Russakovsky *et al.*, "Imagenet large scale visual recognition challenge," *Int. J. Comput. Vis.*, vol. 115, no. 3, pp. 211–252, 2015.
[8] R. Girshick, J. Donahue, T. Darrell, and J. Malik, "Rich feature hierarchies for accurate object detection and semantic segmentation," in *Proc. IEEE Conf. Comput. Vis. Pattern Recognit.*, Jun. 2014, pp. 580–587.
[9] O. Ronneberger, P. Fischer, and T. Brox, "U-Net: Convolutional networks for biomedical image segmentation," in *Proc. Int. Conf. Med. Image Comput. Comput.-Assisted Intervention*, 2015, pp. 234–241.
[10] N. Ibtehaz and M. S. Rahman, "MultiResUNet: Rethinking the U-Net architecture for multimodal biomedical image segmentation," *Neural Netw.*, vol. 121, pp. 74–87, 2020.
[11] Y. Wang, "Cognitive foundations of knowledge science and deep knowledge learning by cognitive robots," in *Proc. 16th IEEE Int. Conf. Cogn. Inform. Cogn. Comput.*, Oxford, U.K., Jul. 2017, p. 5.
[12] A. M. Alzahed, S. M. Mikki, and Y. M. M. Antar, "Nonlinear mutual coupling compensation operator design using a novel electromagnetic machine learning paradigm," *IEEE Antennas Wireless Propag. Lett.*, vol. 18, no. 5, pp. 861–865, May 2019.
[13] X. Guo, W. Li, and F. Iorio, "Convolutional neural networks for steady flow approximation," in *Proc. 22nd ACM SIGKDD Int. Conf. Knowl. Discovery Data Mining*, New York, NY, USA, 2016, pp. 481–490.
[14] J. Tompson, K. Schlachter, P. Sprechmann, and K. Perlin, "Accelerating Eulerian fluid simulation with convolutional networks," in *Proc. Int. Conf. Mach. Learn.*, 2017, vol. 70, pp. 3424–3433.

[15] X. Xiao, Y. Zhou, H. Wang, and X. Yang, "A novel CNN-based Poisson solver for fluid simulation," *IEEE Trans. Vis. Comput. Graph.*, vol. 26, no. 3, pp. 1454–1465, Mar. 2020.
[16] W. Tang *et al.*, "Study on a Poisson's equation solver based on deep learning technique," in *Proc. IEEE Elect. Des. Adv. Packag. Syst. Symp.*, Haining, China, Dec. 2017, pp. 1–3, doi: 10.1109/EDAPS.2017.8277017.
[17] T. Shan *et al.*, "Study on a 3D Poisson's equation solver based on deep learning technique," in *Proc. IEEE Int. Conf. Comput. Electromagn.*, Chengdu, China, 2018, pp. 1–3.
[18] H. Yao, L. Jiang, and Y. Qin, "Machine learning based method of moments (ML-MoM)," in *Proc. IEEE Int. Symp. Antennas Propag. USNC/URSI Nat. Radio Sci. Meet ing*, San Diego, CA, USA, 2017, pp. 973–974, doi: 10.1109/APUSNCURSINRSM.2017.8072529.
[19] H. M. Yao and L. J. Jiang, "Machine learning based neural network solving methods for the FDTD method," in *Proc. IEEE Int. Symp. Antennas Propag. USNC/URSI Nat. Radio Sci. Meeting*, Boston, MA, USA, Jul. 2018, pp. 2321–2322.
[20] H. M. Yao and L. Jiang, "Machine-learning-based PML for the FDTD method," *IEEE Antennas Wireless Propag. Lett.*, vol. 18, no. 1, pp. 192–196, Jan. 2019.
[21] A. Khan, V. Ghorbanian, and D. Lowther, "Deep learning for magnetic field estimation," *IEEE Trans. Magn.*, vol. 55, no. 6, pp. 1–4, Jun. 2019.
[22] J. Xiao, J. Li, Y. Chen, F. Han, and Q. H. Liu, "Fast electromagnetic inversion of inhomogeneous scatterers embedded in layered media by born approximation and 3-D U-Net," *IEEE Geosci. Remote Sens. Lett.*, to be published. doi: 10.1109/LGRS.2019.2953708.
[23] Z. Wei and X. Chen, "Deep-learning schemes for full-wave nonlinear inverse scattering problems," *IEEE Trans. Geosci. Remote Sens.*, vol. 57, no. 4, pp. 1849–1860, Apr. 2019.
[24] H. M. Yao, W. E. I. Sha, and L. Jiang, "Two-step enhanced deep learning approach for electromagnetic inverse scattering problems," *IEEE Antennas Wireless Propag. Lett.*, vol. 18, no. 11, pp. 2254–2258, Jul. 2019.
[25] K. He, X. Zhang, S. Ren, and J. Sun, "Deep residual learning for image recognition," in *Proc. IEEE Conf. Comput. Vis. Pattern Recognit.*, Jun. 2016, pp. 770–778.
[26] M. Hestenes and E. Stiefel, "Method of conjugate gradients for solving linear systems," *J. Res. Nat. Bur. Standards*, vol. 49, no. 6, pp. 409–436, 1952.
[27] V. Simoncini and D. B. Szyld, "Recent computational developments in Krylov subspace methods for linear systems," *Numer. Linear Algebra Appl.*, vol. 14, no. 1, pp. 1–59, 2007.

Shutong Qi is a senior student with the School of Electronics and Information Engineering, Beihang University, Beijing, China.

Since 2018, he has been a Member of the Institute of EMC Technology under the supervision of Prof. Qiang Ren. His current research interests include electromagnetics, machine learning, and human–computer interaction.

Yinpeng Wang is currently working toward the undergraduate degree in electrical engineering in the School of Electronics and Information Engineering, Beihang University, Beijing, China.

His current research interests include electromagnetic scattering, inverse scattering, deep learning, and multiphysics modeling.

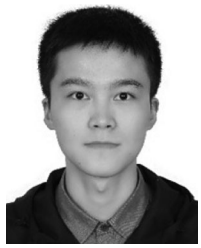

Yongzhong Li is currently working toward the undergraduate degree in electrical engineering in the School of Electronics and Information Engineering, Beihang University, Beijing, China.

His current research interests include multiphysics modeling, deep learning, as well as flexible electronics in terms of nanomaterials and nanophotonics.

Xuan Wu received the B.S. degree in electronics and information engineering from Beihang University, Beijing, China, in 2019, where she is currently working toward the postgraduate degree with the School of Electronics and Information Engineering.

Her current research interests include computational electromagnetics, electromagnetic compatibility, and dispersive materials.

Qiang Ren received the B.S. degree from Beihang University, Beijing, China, in 2008, the M.S. degree from the Institute of Acoustics, Chinese Academy of Sciences, Beijing, China, in 2011, and the Ph.D. degree from Duke University, Durham, NC, USA, in 2015, all in electrical engineering.

From 2016 to 2017, he was a Postdoctoral Researcher with the Computational Electromagnetics and Antennas Research Laboratory (CEARL), Pennsylvania State University, University Park, PA, USA. In September 2017, he joined the School of Electronics and Information Engineering, Beihang University, as an "Excellent Hundred" Associate Professor. His current research interests include numerical methods for multiscale and multiphysics modeling, inverse scattering, and parallel computing.

Dr. Ren was the recipient of the Young Scientist Award of the 2018 International Applied Computational Electromagnetics Society (ACES) Symposium in China.

Yi Ren (Member, IEEE) was born in Anhui, China, in 1982. He received the B.S. degree from Anhui University, Hefei, China, in 2004 and the Ph.D. degree from the University of Electronic Science and Technology of China (UESTC), Chengdu, China, in 2009, respectively, both in electrical engineering.

Since 2009, he has been an Electromagnetic Compatibility Engineer with Chongqing Jinmei Inc., Shapingba, China. Since 2011, he has been with the Chongqing University of Posts and Telecommunications (CQUPT), Chongqing, China, where he is currently a Professor of electronic engineering. From 2014 to 2015, he was a Postdoctoral Research Scholar with Duke University, Durham, NC, USA. His current research interests include computational electromagnetics and electromagnetic compatibility.